Soil Dynamics and Earthquake Engineering 173 (2023) 108115

Contents lists available at ScienceDirect

Soil Dynamics and Earthquake Engineering

journal homepage: www.elsevier.com/locate/soildyn

Bayesian analysis-based ground motion prediction equations for earthquake input energy

Edén Bojórquez [a], Sonia E. Ruiz [b], Ali Rodríguez-Castellanos [c,*], Miguel A. Orellana [b], Alfredo Reyes-Salazar [a], Juan Bojórquez [a]

[a] Facultad de Ingeniería, Universidad Autonoma de Sinaloa, Calzada de las Américas y B, Universitarios s/n, C.P. 80040, Culiacán, Sinaloa, Mexico
[b] Instituto de Ingeniería, Universidad Nacional Autonoma de Mexico, Ciudad Universitaria Coyoacán, C.P. 04510, CDMX, Mexico
[c] Escuela de Ingeniería, Universidad Autonoma de Sinaloa, Av. Ejercito mexicano y Universidad s/n, C.P. 82017, Mazatlan, Sinaloa, Mexico

ARTICLE INFO

Keywords:
GMPEs
Subduction earthquakes
Seismic input energy
Bayesian regression
Correlation coefficients
PSHA
Intensity measures

ABSTRACT

Earthquake energy-based procedures offer a promising alternative for seismic evaluation and earthquake-resistant design of structures. Accurate determination of earthquake energy demand and the provision of an adequate energy supply to the structural system are crucial for this approach. This is where the utilization of ground motion prediction equations (GMPEs) becomes essential in achieving accurate assessment of seismic demands on structures. However, most GMPEs primarily focus on determining spectral accelerations. This study proposes a methodology to derive GMPEs by combining the Fourier amplitude spectrum, the elastic input energy spectrum, and Bayesian regression analysis. These GMPEs estimate energy-based spectral values for interplate and intraslab earthquakes recorded in the firm ground of Mexico City. Furthermore, a mathematical expression is devised to determine correlation coefficients between energy-based spectral values for interplate and intraslab earthquakes, expanding the GMPEs' applicability. Finally, a probabilistic seismic hazard analysis is conducted using the proposed GMPEs and the correlation model.

1. Introduction

Most current seismic design codes present force-based seismic design procedures [1–3]; however, these methods may not ensure satisfactory structural behavior during significant earthquake events [4]. Recognizing this limitation, recent earthquake-resistant design methodologies have shifted towards the performance-based seismic design philosophy, which prioritize the control of specific structural response parameters to achieve effective damage control in earthquake-resistant structures [5]. This approach operates under the assumption that seismic damage in structural systems is better correlated with displacements rather than forces. It uses the displacement demand of structures as a performance criterion. However, it is widely acknowledged that structural damage during earthquakes depends not only on the maximum displacement demand but also on the seismic load history, the energy dissipation capacity of structural components, and the earthquake duration [6–8]. In light of this, several studies have proposed energy-based procedures as a comprehensive solution for seismic design and assessment of structures [9–16]. These procedures provide an alternative to current design methodologies, offering a more holistic approach to seismic design by considering the seismic load history, energy dissipation capacity, and earthquake duration.

In the context of energy-based design procedures, it is necessary to estimate the seismic demand in terms of input energy and the energy dissipation capacity of the structural system. Consequently, the initial step in energy-based methods involves defining the earthquake demand imposed on structures by utilizing energy parameters that effectively characterize the potential of seismic events, *i.e.*, ground motion intensity measures (IMs) based on energy considerations. In this regard, earthquake input energy (E_I) has been widely used as an IM to represent the earthquake demand, which refers to the energy imparted to a structure during ground motions [17]. It is a comprehensive measure that takes into account factors such as earthquake duration, cumulative damage, and it has shown to be a reliable predictor of the structural response [12,14,15,18–20].

Ground-motion prediction equations (GMPEs) have been proposed as a means to estimate the earthquake input energy, specifically expressed in terms of the equivalent velocity (V_{EI}). For instance,

* Corresponding author.
E-mail address: arodriguezca@uas.edu.mx (A. Rodríguez-Castellanos).

https://doi.org/10.1016/j.soildyn.2023.108115
Received 19 April 2023; Received in revised form 21 June 2023; Accepted 1 July 2023

Chapman [21] and Gong and Xie [22] developed V_{EI} prediction equations by utilizing ground motion records from Western North America. They employed a two-step regression analysis to determine the unknown coefficients of the attenuation relationship [23]. Similarly, Danciu and Tselentis [24] established a V_{EI} attenuation relationship for Greece using the mixed-effect model to determine the regression coefficients of the adopted predictive equation. More recently, Cheng et al. [25] and Alıcı and Sucuoğlu [26] utilized ground motion records from the Next Generation Attenuation (NGA) project database to propose GMPEs for V_{EI}. They employed nonlinear regression analysis to determine the appropriate regression coefficients associated with the prediction equations. It is worth noting that the aforementioned GMPEs were developed based on extensive datasets comprising hundreds of ground motion records. However, a challenge arises when the seismic data available is limited, as extrapolating ground-motion prediction equations derived for specific seismic environments may yield inaccurate outcomes.

In this study, a formulation is presented based on the relationship between the Fourier amplitude spectrum and the elastic input energy spectrum, in conjunction with Bayesian regression analyses. The procedure is applied to derive GMPEs for the firm ground of Mexico City, aiming to estimate the input energy converted to an equivalent velocity corresponding to interplate and, separately, intraslab seismic events. The presented methodology significantly contributes to the first task in the energy-based seismic design approach, which is defining the earthquake demand in terms of energy. Furthermore, to extend the applicability of the derived GMPEs, correlation coefficients are computed between V_{EI} spectral values. These correlations are useful for defining the joint distribution of V_{EI} spectral values at multiple periods, allowing for various seismic hazard applications. For instance, the proposed GMPEs and correlation model can be used in vector-valued probabilistic seismic hazard analysis [27], simulation of response spectra for specific earthquake scenarios [28], and the development of custom ground-motion prediction equations [29,30]. Moreover, they can be applied in probabilistic seismic hazard analysis (PSHA) with improved scalar intensity measures [31] or conditional mean spectra [31,32]. To illustrate the practical application of the methodology, a probabilistic seismic hazard analysis was performed using two intensity measures. This analysis serves as an example of how the derived GMPEs and correlation model can be employed to assess the seismic hazard at a specific site.

2. State-of-the-art on energy-based seismic design

2.1. Relative seismic input-energy

The objective is to present a methodology for developing ground-motion prediction equations, also known as attenuation relationships, that can accurately predict the input energy associated with interplate and intraslab seismic events (which will be further characterized in subsequent sections). This approach is specifically applied to the firm ground of Mexico City. In this regard, the subsoil within the city is classified into three zones: the lakebed zone (soft soil), characterized by a clay deposit that exhibits high compressibility and water content; the transition zone, which comprises alluvial sandy and silty layers occasionally interspersed with clay layers; and the hill zone (firm ground), distinguished by a surface layer consisting of lava flows and volcanic tuffs. The shear-wave velocities in the upper 30 m of these zones are approximately 50–100 m/s, 750 m/s, and 250 m/s, respectively [33].

The focus of interest lies in the concept of relative seismic input-energy as discussed in the literature. To adequately define this energy concept, the equation of motion for a single degree of freedom (SDOF) system subjected to ground acceleration ($\ddot{x}_g$) is considered:

$$m\ddot{x} + c\dot{x} + fs(x,\dot{x}) = -m\ddot{x}_g \tag{1}$$

where x represents the relative displacement concerning the ground, and dots over x indicate the derivatives with respect to time. m represents the mass, c the damping coefficient, and fs the restoring force of the system. Following the derivation for the relative input-energy proposed by Uang and Bertero [18], integration of Eq. (1) with respect to x yields the following expression:

$$\int m\ddot{x}dx + \int c\dot{x}dx + \int fs(x,\dot{x})dx = -m\int \ddot{x}_g dx \tag{2}$$

Then, Eq. (2) gives the energy balance equation, which can be rewritten as:

$$E_k + E_D + E_s + E_H = E_I = -m\int \ddot{x}_g dx \tag{3}$$

where E_k denotes the relative kinetic energy, E_D is the viscous damping energy, E_s is the elastic strain energy, E_H is the hysteretic energy, and E_I is the relative earthquake input-energy. Physically, E_I represents the work done by the equivalent lateral force ($-m\ddot{x}_g$) on the fixed base system [18]. Henceforth, the relative input-energy will be referred to as earthquake input-energy, E_I. Additionally, for eliminating the mass term, the input-energy can be related to an equivalent velocity, which serves as the seismic intensity measure (IM) employed in the development of the GMPEs. This equivalent velocity is represented as follows:

$$V_{EI} = \sqrt{2E_I/m} \tag{4}$$

2.2. Input-energy from the Fourier spectrum

Research has demonstrated that the elastic input-energy spectrum can be obtained through the Fourier amplitude spectrum [34]. Based on Eq. (3), the following relationship is established [34]. :

$$\frac{E_I}{m} = -\int_{-\infty}^{\infty} \ddot{x}_g(t)dx \tag{5}$$

Considering the relationship $dx = dt(dx/dt) = \dot{x}(t)dt$, Eq. (5) can be expressed as:

$$\frac{E_I}{m} = -\int_{-\infty}^{\infty} \ddot{x}_g(t)\dot{x}dt \tag{6}$$

Then, by employing the definition of the Fourier transform, the velocity of the SDOF system $\dot{x}(t)$ can be written as follows:

$$\dot{x}(t) = \frac{1}{2\pi}\int_{-\infty}^{\infty} A(\omega)H_V(\omega;\Omega,\xi)e^{i\omega t}d\omega \tag{7}$$

where ω represents the frequency of the SDOF system, $A(\omega)$ denotes the Fourier transform of $\ddot{x}_g$ and $H_V(\omega;\Omega,\xi)$ is transfer function of $\dot{x}$ relative to $\ddot{x}_g$. By substituting Eq. (7) into Eq. (6) and rearranging the integrals accordingly, the following expression is obtained:

$$\frac{E_I}{m} = -\frac{1}{2\pi}\int_{-\infty}^{\infty} A(\omega)H_V(\omega;\Omega,\xi)\int_{-\infty}^{\infty} \ddot{x}_g(t)e^{i\omega t}d\omega dt \tag{8}$$

The second integral on the right side of Eq. (8) is the Fourier transform of $\ddot{x}_g$ at frequency $(-\omega)$; therefore, $A(-\omega) = \int_{-\infty}^{\infty} \ddot{x}_g(t)e^{i\omega t}dt$. Finally, the input-energy is given by:

$$\frac{E_I}{m} = -\frac{1}{\pi}\int_0^{\infty} |A(\omega)|^2 F(\omega)d\omega \tag{9}$$

where $F(\omega)$ is the Real part of $H_V(\omega;\Omega,\xi)$, which can be computed as a step-by-step derivation of the input-energy from the Fourier spectrum [34,35]:

$$F(\omega) = Re[H_V(\omega;\Omega,\xi)] = -\frac{2\xi\Omega\omega^2}{\left(\Omega^2-\omega^2\right)^2+(2\xi\omega\Omega)^2} \tag{10}$$

The interest lies in the equivalent velocity of energy, V_{EI}, thus, substituting Eq. (9) into Eq. (4) yields:

$$V_{EI} = \sqrt{2\left[-\frac{1}{\pi}\int_0^\infty |A(\omega)|^2 F(\omega) d\omega\right]} \tag{11}$$

Please note that $A(\omega)$ is the only parameter that still needs to be defined, which will be addressed later, in order to calculate the V_{EI} response spectrum for a specific seismic event. However, it is important to emphasize that the ultimate objective is to propose an attenuation relationship for V_{EI} as a function of the vibration period, similar to what is done with other GMPEs.

3. Bayesian regression analysis

Formerly, the attenuation relationships were developed using ordinary least-squares regression analysis. However, this method has been found to have shortcomings, leading to the emergence of advanced techniques [23,36–38]. In this sense, Bayesian approaches have been demonstrated to yield more accurate results compared to traditional and innovative counterparts, particularly when there is limited seismic data available [39–41]. The appeal of the Bayesian approach lies in the fact that it requires the prior definition of expected values for the coefficients of the selected functional form, without the reliance on actual seismic data. In other words, it is necessary to estimate in advance what the model coefficient values should be based on existing seismological knowledge. This initial step involves determining what is known in Bayesian terminology as the *prior* coefficients for the chosen GMPEs. Subsequently, in the second step, once the *prior* coefficients have been defined, they are updated by incorporating the available seismic data, resulting in the *posterior* coefficients. Hence, it is crucial to establish a mathematical relationship to model the attenuation of interplate and intraslab events before defining the *prior* and *posterior* coefficients. With this in mind, Eqs. (12) and (13) represent the adopted functional forms for predicting the median values of V_{EI} associated with interplate and intraslab rupture mechanisms.

$$lnY(T_n) = \alpha_1(T_n) + \alpha_2(T_n)M_w + \alpha_3(T_n)lnR + \alpha_4(T_n)R + \varepsilon(T_n) \tag{12}$$

$$lnY(T_n) = \alpha_1(T_n) + \alpha_2(T_n)(M_w-6) + \alpha_3(T_n)(M_w-6)^2 + \alpha_4(T_n)lnR + \alpha_5(T_n)R + \varepsilon(T_n) \tag{13}$$

where Y is the quadratic mean of the horizontal ground motion components of V_{EI} (in cm/s) for a given SDOF period system T_n, M_w is the moment magnitude, R is the closest distance to fault surface (according to the circular finite-source model [41]), α_i are the coefficients to be estimated by the regression analysis, and ε is the random error assumed to be normally distributed.

On the other hand, both Equations (12) and (13) are utilized to estimate the V_{EI} response spectra for interplate and intraslab earthquakes, as illustrated in Figs. 6 and 7 further on. Additionally, it is worth noting that although these prediction models do not incorporate specific information associated with seismic events in subduction zones (such as back arc and fore arc conditions), they have demonstrated a strong ability to accurately predict spectral acceleration values. This consistent track record significantly enhances their reliability. Consequently, the selection of the predictive equations was solely guided by the findings of previous studies that have successfully employed these specific prediction equations [39–44].

3.1. Prior regression coefficients

To estimate the *prior* coefficients in the aforementioned equations, let's consider Eq. (11). It is important to note that $A(\omega)$ is the only parameter that remains to be defined. In this regard, the Fourier amplitude spectrum can be characterized through the following seismological model, along with typical geometrical and anelastic attenuation functions for far-field approximation [45]:

$$A(\omega) = \frac{R_P F_s P}{4\pi\rho_s\beta^3}\frac{S(\omega,M_w)}{R}G(R)e^{-\omega R/2\beta Q(\omega)} \tag{14}$$

where R_P represents the average radiation pattern, F_S takes into account the free-surface amplification, P considers the partition of energy in the two horizontal components, ρ_s denotes the density of the medium through which the wave travels, while β represents the shear wave velocity. $S(\omega,M_w)$ represents the Brunes's ω^2 source spectrum model [46] where the corner frequency was determined based on the studies conducted by Rodríguez-Pérez et al. [47] and Garcia et al. [48] for interplate and intraslab seismic events, respectively. Additionally, $G(R)$ represents the geometrical spreading, modeled as described in Garcia et al. [49] and Ordaz et al. [39] for interplate and intraslab earthquakes, respectively. $Q(\omega)$ refers to the quality factor, which incorporates the effects of anelastic absorption and scattering of the seismic waves. The values for the quality factor were inferred from Garcia et al. [49] and Garcia et al. [48] for interplate and intraslab earthquakes, respectively.

By substituting Eq. (14) into Eq. (11) and fixing the distance, R [44,50], while subsequently varying the magnitude values M_w for interplate events (ranging from 6.1 to 8.1) and intraslab events (ranging from 5.0 to 7.5), within a range of vibration periods between 0.01 s and 10 s, it becomes theoretically possible to compute the 5% damped V_{EI} response spectra. This process allowed for the generation of a synthetic sample of V_{EI} response spectra solely based on seismological concepts, which was valuable for determining the *prior* expected values for the coefficients $E'[\alpha_i(T)]$ in Eqs. (12) and (13).

Having obtained the V_{EI} response spectra, the *prior* expected values $E'[\alpha_1(T)]$ and $E'[\alpha_2(T)]$ for Eq. (12) and $E'[\alpha_1(T)]$ to $E'[\alpha_3(T)]$ for Eq. (13) were estimated through ordinary least-squares regression analysis. Additionally, it was necessary to assign *prior* uncertainties to these coefficients. Specifically, for both functional forms Eqs. (12) and (13), the prior standard deviation $\sigma'[\alpha_1(T)]$ was assumed to be sufficiently large to account for site effects. Meanwhile, the prior standard deviations $\sigma'[\alpha_2(T)]$ for Eq. (12), and $\sigma'[\alpha_2(T)]$ and $\sigma'[\alpha_3(T)]$ for Eq. (13), were estimated as $\sigma'[\alpha_i(T)/1.7]$, following the approach proposed by Ordaz et al. [39].

Moreover, it should be noted that the regression coefficients $\alpha_3(T)$ and $\alpha_4(T)$, which correspond to Eqs. (12) and (13) respectively, are equivalent. In this regard, these regression coefficients govern the geometrical spreading $G(R)$, which is significantly constrained from a theoretical perspective [39]. The value of this parameter typically ranges from −0.5 to −1.3 [44,50–52]. In this sense, Ordaz et al. [39], compared the Bayesian solutions assuming $E'[\alpha_3(T)]$ = -1.0 and $E'[\alpha_3(T)] = -0.5$. The results indicated that the *posterior* expected values for the remaining coefficients depend on the *prior* expected value selection, but the differences were not significant and did not impact the overall outcome. Consequently, in this study, the *prior* expected values were stablished as $E'[\alpha_3(T)] = -1.0$ and $E'[\alpha_4(T)] = -1.0$ for Eqs. (12) and (13), respectively. Furthermore, the quality factor model $Q(\omega)$ employed in this study was developed assuming a geometrical spreading coefficient equivalent to −1.0 [48]. Additionally, the prior standard deviations for $\sigma'[\alpha_3(T)]$ and $\sigma'[\alpha_4(T)]$ of both functional forms, Eq. (12) and Eq. (13), also needed to be defined. For this purpose, a variance was assumed to be sufficiently small to ensure a nearly constant behavior for the *posterior* expected values $E''[\alpha_3(T)]$ and $E''[\alpha_4(T)]$ [44,50].

As in the previous case, the regression coefficients $\alpha_4(T)$ and $\alpha_5(T)$ corresponding to Eqs. (12) and (13) respectively, are also identical. In this case, the *prior* expected values, $E'[\alpha_4(T)]$ and $E'[\alpha_5(T)]$, were determined based on the approach proposed by Reyes [50], which utilizes spectral ratios between V_{EI} response spectra computed using Eqs. (11) and (14) at two different distances (R_1 and R_2). In this sense, $E'[\alpha_4(T)]$ and $E'[\alpha_5(T)]$ can be computed using Eq. (15) as provided by Reyes [50]. Furthermore, for the prior standard deviations, $\sigma'[\alpha_4(T)]$ and $\sigma'[\alpha_5(T)]$, a sufficiently high variance was adopted to yield the optimal solution for the regression analysis [44,50]. This variance selection aims to capture the uncertainties associated with these coefficients and ensure robust results in the analysis.

$$E^{'}\left[\alpha_{4,5}\right] = \frac{\ln(V_{EI1}/V_{EI2}) - E^{'}\left[\alpha_{3,4}\right]\ln\,(R_1/R_2)}{R_1 - R_2} \tag{15}$$

Finally, the *prior* expected value ($E'[\sigma(T)]$) for the standard error needed to be specified. In this respect, it was assumed as $E'[\sigma(T)] = 0.7$ based on the uncertainties obtained from other GMPEs [40,42,44,50], and its standard deviation was taken as $\sigma'[\sigma(T)/1.7]$.

3.2. Posterior regression coefficients

Once the *prior* expected values for the coefficients corresponding to Eqs. (12) and (13) were generated, the estimation of the corresponding *posterior* expected values was carried out through Bayesian regression analysis. For this analysis, studies from Ordaz et al. [39] and Reyes [50] were used as reference frameworks. Thus, readers are encouraged to consult those references for further details. Broadly speaking, the Bayesian approach updates the *prior* expected values by incorporating the available seismic data, resulting in *posterior* expected values for the coefficients of the selected functional form. The *posterior* values represent the final coefficients associated with the GMPEs.

4. Selected recorded accelerograms

The compiled ground motions were obtained from the CU accelerometer station, which represents firm ground conditions in Mexico City. The epicenters of these seismic events are illustrated in Fig. 1. In this regard, the selected records were provided by the Strong Motion Network of the Institute of Engineering at UNAM, Mexico (RAII-UNAM), as shown in Table 1 and Table 2. All the records underwent linear baseline correction and were subjected to a Butterworth bandpass filter. The cut-off frequencies of the bandpass filter varied for each ground motion and were selected from Fourier spectra. The minimum and maximum cut-off frequencies for the entire set of signals were 0.1 Hz and 25 Hz, respectively. Additionally, a ground motion duration corresponding to 2.5% and 97.5% of the Arias intensity was taken into consideration.

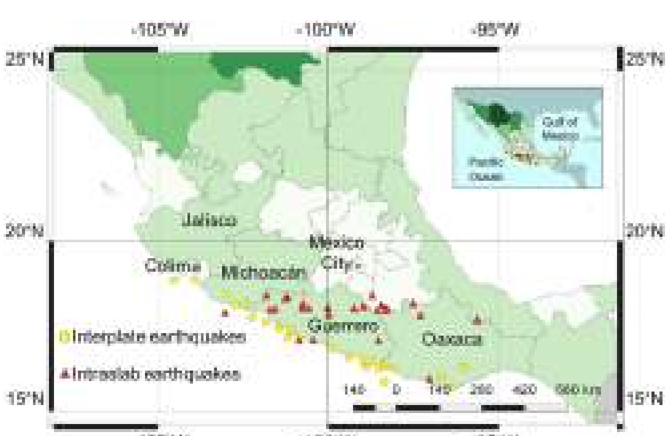

Fig. 1. Map of southern of Mexico showing epicenters of Interplate (circles) and Intraslab earthquakes (triangles) used in the present study.

Table 1
Interplate seismic events recorded in CU station.

Date	M_w	R (km)	Depth (km)	Date	M_w	R (km)	Depth (km)
23/08/1965	7.8	466	16	15/05/1993	6.0	320	20
02/08/1968	7.4	326	33	24/10/1993	6.7	310	19
19/03/1978	6.4	285	16	14/09/1995	7.3	320	22
29/11/1978	7.8	414	19	09/10/1995	8.0	530	27
14/03/1979	7.6	287	20	15/07/1996	6.6	301	20
25/10/1981	7.3	330	20	19/07/1997	6.7	394	15
07/06/1982	6.9	304	15	03/02/1998	6.3	509	33
07/06/1982	7.0	303	15	09/08/2000	6.5	380	33
19/09/1985	8.1	295	15	01/01/2004	6.0	323	15
21/09/1985	7.6	318	15	20/03/2012	7.4	329	16
30/04/1986	7.0	409	16	18/04/2014	7.2	304	10
25/04/1989	6.9	290	19	08/05/2014	6.4	298	17
31/05/1990	6.1	304	21				

Table 2
Intraslab seismic events recorded in CU station.

Date	M_w	R (km)	Depth (km)	Date	M_w	R (km)	Depth (km)
06/07/1964	7.3	217	55	21/06/1999	6.3	310	53
07/06/1976	6.4	310	57	30/09/1999	7.4	415	47
24/10/1980	7	169	70	21/07/2000	5.9	146	50
05/08/1993	5.2	237	54	20/02/2006	5.2	191	56
23/02/1994	5.8	278	75	11/08/2006	6	228	58
06/05/1994	5.2	160	62	13/04/2007	6	244	43
23/05/1994	6.2	209	50	28/04/2008	5.8	195	56
10/12/1994	6.4	300	50	22/05/2009	5.6	168	59
11/01/1997	7.1	377	40	11/12/2011	6.5	176	55
03/04/1997	5.2	154	52	16/06/2013	5.9	103	52
22/05/1997	6.5	300	54	29/07/2014	6.4	432	110
20/04/1998	5.9	246	64	20/03/2015	5.4	178	61
15/06/1999	6.9	218	61	19/09/2017	7.1	105	57

The compiled ground-motion records are associated with interplate and intraslab earthquakes and have been classified based on their focal mechanism. Interplate earthquakes occur along the Cocos-North American plate boundary, specifically along Mexico's Pacific coastline, at distances exceeding 300 km from Mexico City (see Fig. 1). These earthquakes involve rupture along a low-angle thrust plane at shallow depths of approximately 15–25 km [33]. In central Mexico, intraslab earthquakes occur within the subducted Cocos plate, typically at depths of 40–80 km, and involve normal faulting. They occur at distances greater than 125 km from Mexico City but within a range of less than

300 km for coastal earthquakes (see Fig. 1) [33]. Additionally, following the directions given by Singh et al. [53], steeply dipping thrust events near the coast were grouped with normal-faulting intraslab earthquakes (see Fig. 1) due to the similarity in their ground motions [48]. For earthquakes with unknown focal mechanisms, depth was used as a criterion: depths less than 40 km were classified as interplate, while depths equal to or greater than 40 km were classified as intraslab [53].

5. Results

5.1. Regression coefficients

For simplicity, the focus is on presenting the regression coefficients obtained from Eq. (12) related to both interplate and intraslab events. Eq. (12) provided the best fit for the actual V_{EI} response spectra corresponding to both earthquakes mechanisms (results for Eq. (13) can be found in Ref. [54]). Tables 3 and 4 show the *posterior* expected values of the regression coefficients and standard deviation (in natural logarithm units) to predict the V_{EI} response spectra for 5% of critical damping corresponding to interplate and intraslab earthquakes, respectively.

Figs. 2 and 3 show a comparison between the *prior* coefficients (continuous line) and the *posterior* coefficients (discontinuous line) obtained from Bayesian regression analysis for interplate and intraslab earthquakes, respectively. These figures demonstrate the physical consistency of the regression coefficients based on the applied seismological theory. Nevertheless, the crucial aspect lies in their ability to accurately predict the actual response spectra. In this regard, the standard deviation provides insight into the accuracy of these predictions, as it reflects the dispersion caused by the ground motion prediction model given the available sample. In this context, for the selected range of periods, the average standard deviation is $\sigma = 0.59$ (as shown in Fig. 2e and 3e). This value was consistent with those reported in previous studies on prediction models for rock sites of Mexico City [39,40,44,50,55].

5.2. Residuals analysis

Figs. 4 and 5 display the residuals for a set of vibration periods associated with interplate and intraslab earthquakes, respectively. The residuals were estimated using Eq. (12) (circles) and Eq. (13) (triangles) as a function of both predictor variablesM_w and R. They were computed as the difference between the natural logarithm of the observed value and the predicted value. A positive value indicates underestimation by the model, while a negative value denotes overestimation. Upon comparing Figs. 4 and 5, it was observed that Eqs. (12) and (13) provide more accurate predictions for intraslab events compared to interplate events. The residuals clearly show a random pattern around the horizontal axis of the two predictor variables, indicating that the attenuation relationships are unbiased with respect to magnitude and distance.

Table 3
Regression coefficients obtained to predict V_{EI} response spectra using Eq. (12), for interplate events.

T_n(s)	α_1	α_2	α_3	α_4	σ
0.01	−8.380	1.242	−0.96	−0.00221	0.65
0.05	−2.808	0.957	−0.97	−0.00310	0.69
0.1	−1.458	1.055	−0.98	−0.00577	0.52
0.5	−0.335	1.292	−0.97	−0.00671	0.62
1.0	−0.318	1.308	−0.98	−0.00469	0.60
2.0	−0.297	1.421	−0.99	−0.00549	0.62
3.0	−0.282	1.384	−0.99	−0.00533	0.65
4.0	−0.268	1.248	−1.01	−0.00329	0.64
5.0	−0.257	1.114	−1.01	−0.00138	0.58
6.0	−0.248	1.083	−1.01	−0.00140	0.59
7.0	−0.241	1.129	−1.00	−0.00293	0.55
8.0	−0.235	1.094	−1.00	−0.00263	0.52
9.0	−0.230	1.095	−1.00	−0.00294	0.52
10	−0.226	1.091	−1.01	−0.00305	0.51

Table 4
Regression coefficients obtained to predict V_{EI} response spectra using Eq. (12), for intraslab events.

T_n(s)	α_1	α_2	α_3	α_4	σ
0.01	−5.649	0.994	−1.04	−0.00311	0.53
0.05	−2.136	0.913	−1.02	−0.00339	0.39
0.1	−1.219	1.085	−1.02	−0.00507	0.46
0.5	−1.868	1.402	−1.01	−0.00267	0.62
1.0	−4.131	1.763	−1.02	−0.00180	0.61
2.0	−6.509	2.054	−1.01	−0.00026	0.67
3.0	−7.725	2.144	−1.01	0.00091	0.66
4.0	−8.724	2.303	−1.00	−0.00010	0.58
5.0	−9.576	2.388	−1.00	0.00048	0.57
6.0	−10.313	2.485	−0.99	0.00013	0.56
7.0	−10.960	2.534	−0.98	0.00034	0.56
8.0	−11.536	2.601	−0.96	−0.00022	0.59
9.0	−12.053	2.666	−0.96	−0.00058	0.63
10	−12.522	2.726	−0.95	−0.00076	0.65

Similar results were observed for the rest of the vibration periods. Based on these findings, it can be reasonably concluded that the predictions align well with the observed data.

5.3. Observed versus predicted V_{EI} response spectra

Figs. 6 and 7 illustrate a comparison between the exact V_{EI} response spectra (thick solid line) and the V_{EI} response spectra estimated using Eq. (12) (dark dashed line) and Eq. (13) (dashed line) for interplate and intraslab ground motion records, respectively. Although some predictions may not be highly accurate, the two proposed attenuation equations generally provide satisfactory estimates for the majority of the analyzed seismic records.

In this sense, they demonstrate effectiveness in predicting ground motions for two of the most devastating earthquakes in Mexico's history: The Michoacán interplate earthquake (shown in Fig. 6) and the Puebla intraslab earthquake (shown in Fig. 7), which occurred in September 19, 1985, and 2017, respectively. Based on these observations, the obtained results can be considered appropriate for engineering purposes.

6. Correlation coefficients between V_{EI} spectral values

As it is well known, the correlation coefficients are useful to define the joint distribution of spectral values at multiple periods, which allows different applications related to seismic hazard analysis. To describe the estimation of the correlation coefficients between V_{EI} spectral values, the following generic prediction equation is considered:

$$ln\ V_{EI}(T_n) = \mu_{ln\ V_{EI}}(M_w, R, \theta, T_n) + \sigma_{ln\ V_{EI}}(T_n)\varepsilon(T_n) \tag{16}$$

where $\mu_{ln\ V_{EI}}(M_w, R, \theta, T_n)$ and $\sigma_{ln\ V_{EI}}(T_n)$ are the predicted mean and the standard deviation of the natural logarithm of V_{EI} at a single vibration period (T_n), given by an attenuation model (*e.g.*, Eq. (12)), as a function of earthquake magnitude (M_w), source-to-site distance (R) and other parameters, (θ). Rearranging Eq. (16) for $\varepsilon(T_n)$, it follows:

$$\varepsilon(T_n) = \frac{ln\ V_{EI}(T_n) - \mu_{ln\ V_{EI}}(M_w, R, \theta, T_n)}{\sigma_{ln\ V_{EI}}(T_n)} \tag{17}$$

where $\varepsilon(T_n)$ represents the difference in standard deviations between the observed lnV_{EI} values and the predicted mean values $\mu_{ln\ V_{EI}}(M_w, R, \theta, T_n)$. These $\varepsilon(T_n)$ values, associated with different vibration periods, are probabilistically correlated. In this study, they were employed to characterize the correlation among V_{EI} spectral values across multiple vibration periods, assuming a normal distribution [29,39,44,56]. Consequently, the Pearson product-moment correlation coefficient was employed to estimate the correlation coefficients at two vibration periods $\varepsilon(T_1)$ and $\varepsilon(T_2)$, as follows:

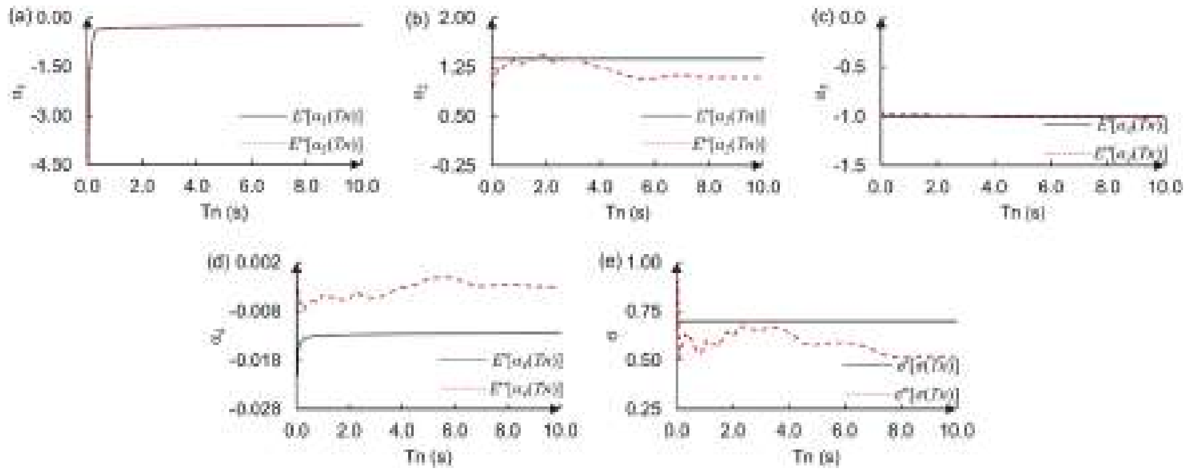

Fig. 2. Prior (solid line) and posterior coefficients (dashed line) for interplate earthquakes.

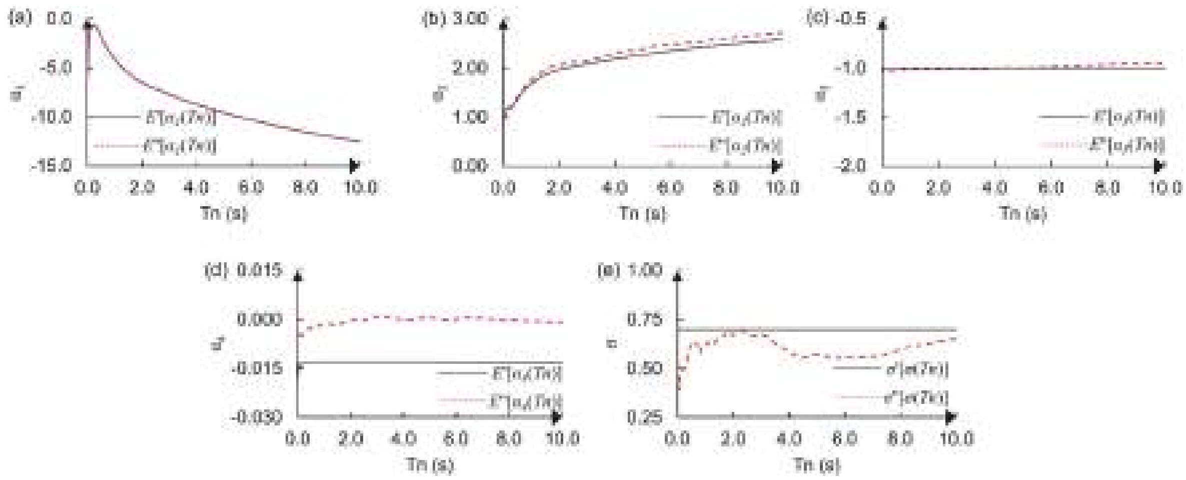

Fig. 3. Prior (solid line) and posterior coefficients (dashed line) for intraslab earthquakes.

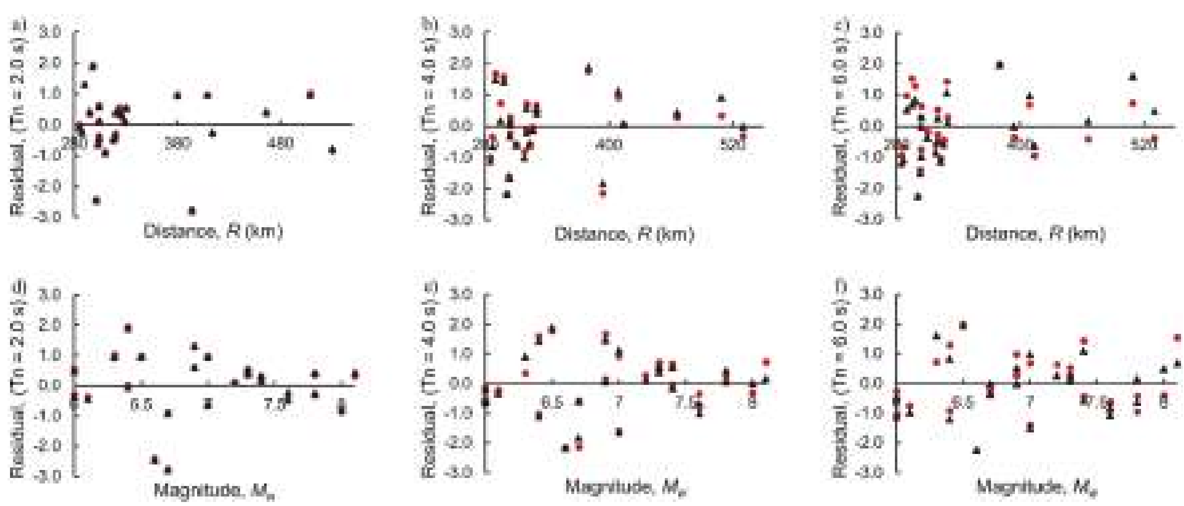

Fig. 4. Residuals for different periods plotted against distance (a–c) and magnitude (d–f) using Eq. (12) (circles) and Eq. (13) triangles, for interplate events.

$$\rho_{\varepsilon(T_1),\varepsilon(T_2)} = \frac{\sum_{i=1}^{n}(\varepsilon_i(T_1) - \overline{\varepsilon(T_1)})(\varepsilon_i(T_2) - \overline{\varepsilon(T_2)})}{\sqrt{\sum_{i=1}^{n}(\varepsilon_i(T_1) - \overline{\varepsilon(T_1)})^2 \sum_{i=1}^{n}(\varepsilon_i(T_2) - \overline{\varepsilon(T_2)})^2}} \tag{18}$$

$\varepsilon_i(T_1)$ and $\varepsilon_i(T_2)$ were evaluated for the *i*-th ground motion record at the vibration periods T_1 and T_2. Meanwhile, $\overline{\varepsilon(T_1)}$ and $\overline{\varepsilon(T_2)}$ represent the sample mean of the residuals corresponding to *n* number of ground motion records. The calculation was repeated for each period pair of

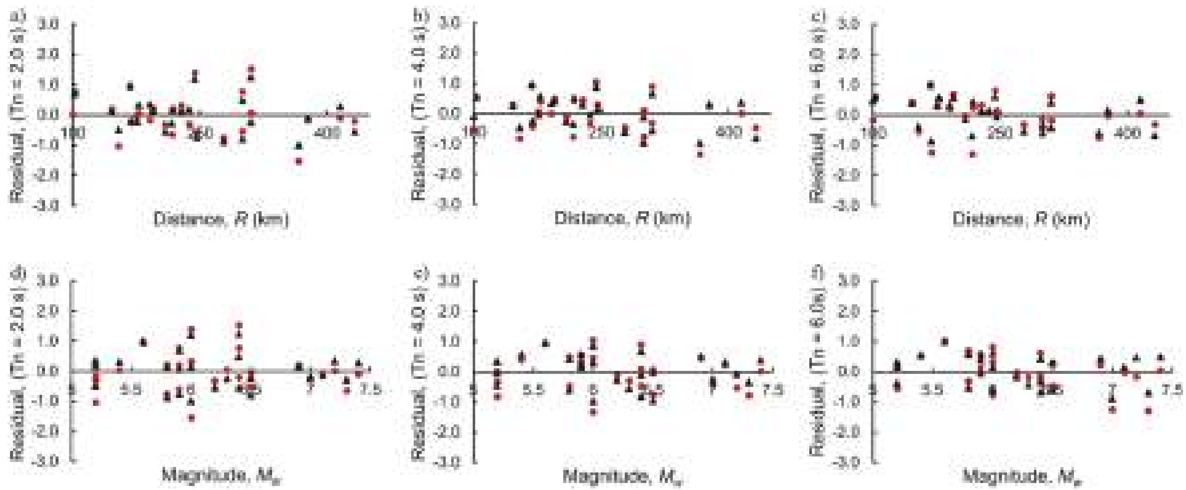

Fig. 5. Residuals for different periods plotted against distance (a–c) and magnitude (d–f) using Eq. (12) (circles) and Eq. (13) triangles, for intraslab events.

interest.

6.1. Correlation coefficients corresponding to interplate and intraslab events

Fig. 8a and b illustrate the correlation coefficients obtained using Eq. (12) for selected period pairs (T_1, T_2), considering the interplate (Table 1) and intraslab (Table 2) ground motion records, respectively. Similarly, Fig. 9a and b presents contour plots showing the computed correlation coefficients as a function of both vibration periods T_1 and T_2. It is observed that the distribution of correlation values differs between interplate (Fig. 9a) and intraslab earthquakes (Fig. 9b). Previous studies have highlighted the dependency of correlation values on the earthquake rupture mechanism [57]. The estimated correlation values range between 0.2 and 1.0 for both earthquake mechanisms, approaching 1.0 when the period pair is closely spaced and decreasing when the period pair is widely separated.

However, even for considerably separated period pairs, high correlation values were observed. For instance, the correlation associated with the period pair $\rho[\epsilon(T_1 = 0.1\text{s}), \epsilon(T_2 = 1.0\text{s})]$ was equal to 0.73 and 0.66 for interplate and intraslab earthquakes, respectively. This finding aligns with previous studies that have examined the correlation between spectral accelerations for the firm ground of Mexico City, which found that correlation values remain high even for well-separated vibration periods [57]. In this context, Carlton and Abrahamson [58] explained that for hard-rock sites with high-frequency content, the correlation between the dominant ground-motion period T_s and periods shorter than T_s remains high and continues to be high even for larger periods than T_s.

6.2. Predictive correlation model for firm ground in Mexico city

The utilization of the previously estimated correlation coefficients poses challenges due to the dimension of each correlation matrix. Therefore, the development of a mathematical expression capable of predicting the observed data depicted in Figs. 8 and 9 becomes advantageous. Hence, the objective was to propose a unified correlation model for both earthquake rupture mechanisms. To achieve this, the correlation model presented in Ref. [57] was adopted. Subsequently, a nonlinear least-squares regression analysis was applied to find the associated parameters of that equation. It is worth noting that the performance of the nonlinear least-squares method is enhanced when the errors for each observed value are of comparable size [59]; however, this is not the case in this scenario. To achieve an approximate constant error, the procedure presented by Baker and Cornell [28] was followed. This involved employing the Fisher z transformation to convert the correlation coefficients into a normally distributed variable denoted as z, thereby improving the performance of the nonlinear regression analysis:

$$z = \frac{1}{2} ln\left(\frac{1+\rho}{1-\rho}\right) \tag{19}$$

where ρ represents the correlation coefficient computed with Eq. (18), and z denotes the transformed variable. Then, the nonlinear least-squares method was applied to the modified values, rather than to the original correlation values estimated with Eq. (18). The analysis was carried out using the following expression:

$$\frac{min}{\beta} \sum_{i=1}^{n} \sum_{j=1}^{n} \left[\frac{1}{2} \ln\left(\frac{1+\rho_{i,j}}{1-\rho_{i,j}}\right) - \frac{1}{2} \ln\left(\frac{1+\widetilde{\rho}_{i,j}(\beta)}{1-\widetilde{\rho}_{i,j}(\beta)}\right) \right] \tag{20}$$

where $\rho_{i,j}$ is the correlation coefficient at the period pair (T_i,T_j), and $\widetilde{\rho}_{i,j}(\beta)$ is the predicted correlation using the proposed predictive equation along with its respective vector of parameters β.

6.3. Predictive correlation model for interplate and intraslab events

The selected predictive correlation equation here was the following [57]:

$$\rho\ \ln[Sa(T_i)], \ln[Sa(T_j)] = \frac{a + bT_{min} + cT_{max}}{1 + dT_{min} + eT_{max}} - fln\left(\frac{T_{max}}{T_{min}}\right) \tag{21}$$

where $T_{\min} = \min(T_1,T_2)$ and $T_{\max} = \max(T_1,T_2)$; the numerical coefficients *a, b, c, d, e* and *f* are shown in Table 5 and Table 6 for interplate and intraslab seismic events, respectively.

Using Eq. (21), Fig. 10a and b shows the correlation coefficients for a selected set of periods T_2, plotted versus T_1 values between 0.1 and 10.0 s, for interplate and intraslab events, respectively. Additionally, Fig. 11a and b presents contour plots illustrating the correlation coefficients as a function of T_1 and T_2 for interplate and intraslab seismic events, respectively. It is worth mentioning that the proposed predictive model estimates the correlation between spectral values corresponding to the quadratic mean of V_{EI} spectral values of the orthogonal horizontal components. In this sense, it has proved that the definition of the spectral acceleration that an attenuation model employs (*i.e.*, the geometric mean or the quadratic mean of spectral values of the two horizontal components of motion) drives to similar spectral acceleration values [59,60]. Therefore, it is reasonable to extend this conclusion to V_{EI}spectral values and assume that the correlation model is applicable regardless of the definition of spectral values used in a given prediction

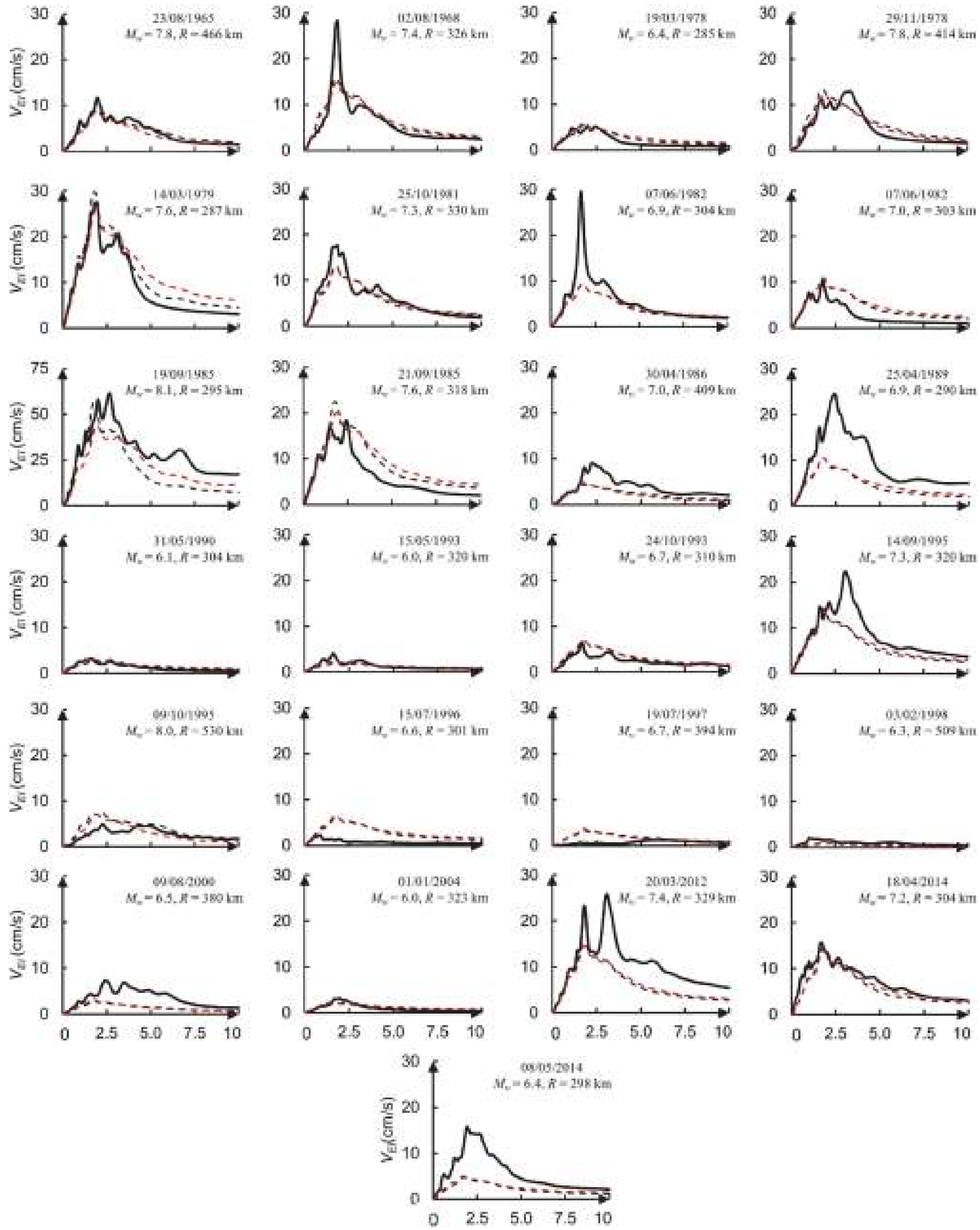

Fig. 6. Observed V_{EI} response spectra for interplate earthquakes (thick solid line) and V_{EI} response spectra estimated using Eq. (12) (dark dashed line) and Eq. (13) (dashed line) employing the coefficients obtained from Bayesian regression analysis.

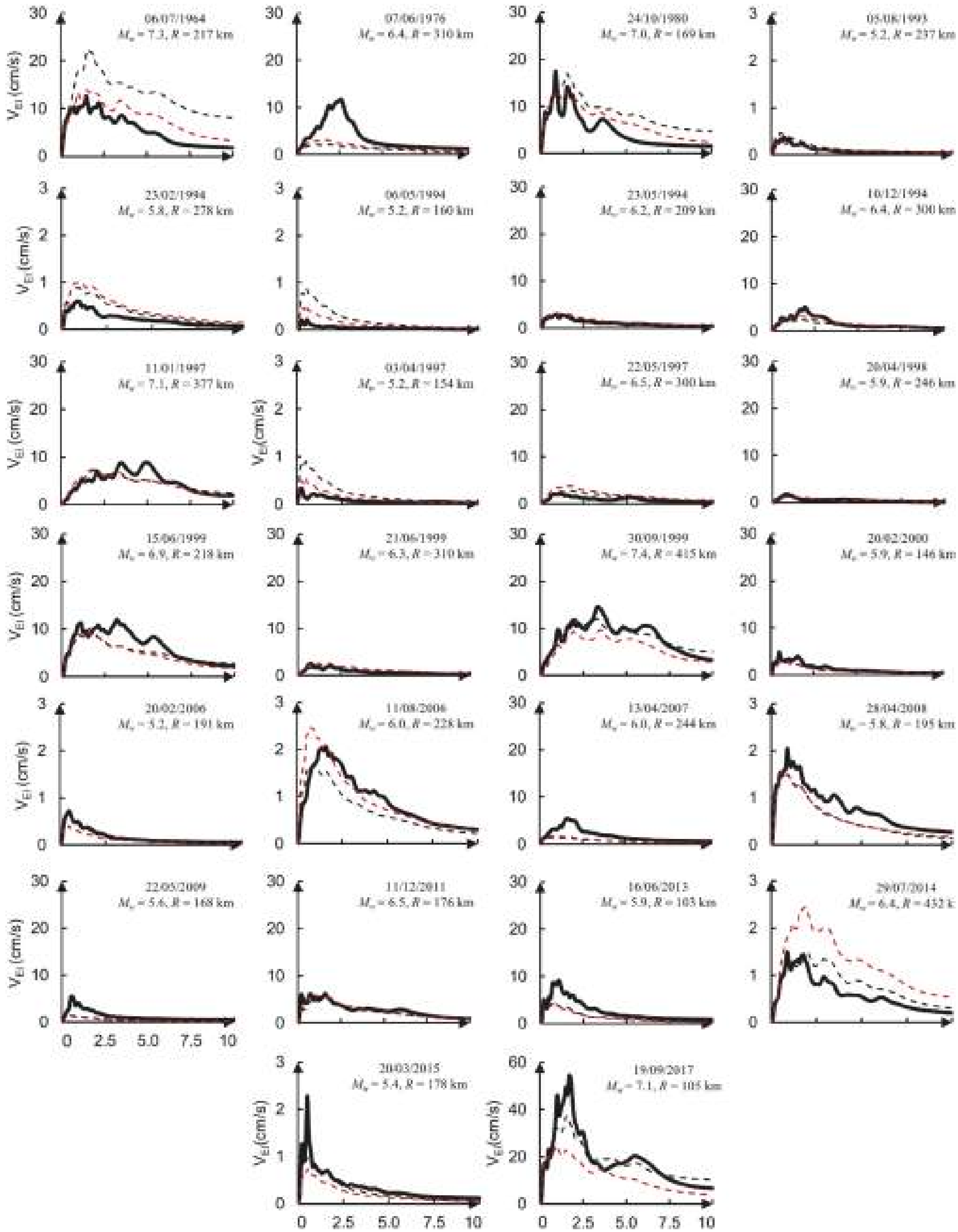

Fig. 7. Observed V_{EI} response spectra for intraslab earthquakes (thick solid line) and V_{EI} response spectra estimated using Eq. (12) (dark dashed line) and Eq. (13) (dashed line) employing the coefficients obtained from Bayesian regression analysis.

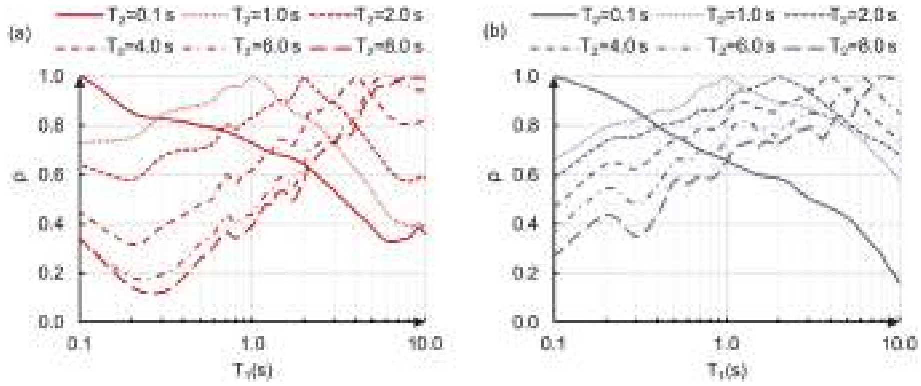

Fig. 8. Correlation coefficients between T_1, and several T_2 values: (a) Interplate and (b) Intraslab earthquakes.

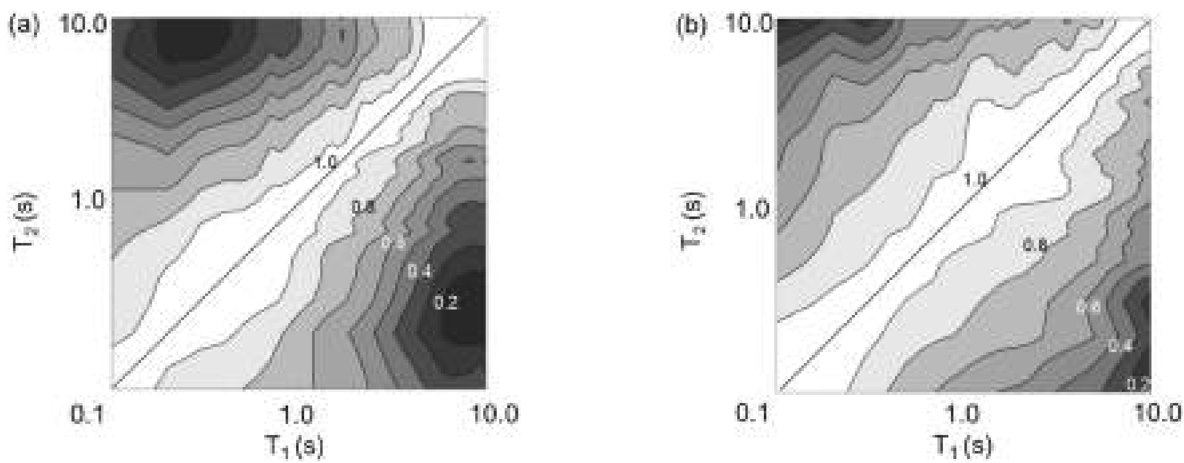

Fig. 9. Contours of correlation coefficients between T_1 and T_2: (a) Interplate and (b) Intraslab earthquakes.

Table 5
Numerical coefficients for interplate predictive correlation equation.

Restriction	*a*	*b*	*c*	*d*	*e*	*f*
	0.9797	1.215	−0.1015	0.8843	0.2446	−0.0047
$T_{max} > 6.1$ and $T_{min} > 1.5$	0.7287	0.3682	−0.1225	0.3482	−0.1454	0.2271
$T_{min} \leq 0.2$	0.9878	−4.9321	0.0001	−4.9933	0.0003	0.1164
$T_{max} > 1.8$ and $T_{min} \leq 0.2$	0.5681	0.983	−0.3736	−1.7321	0.3294	−0.2285

Table 6
Numerical coefficients for intraslab predictive correlation equation.

Restriction	*a*	*b*	*c*	*d*	*e*	*f*
	0.9586	2.2872	−0.1001	2.3046	−0.0352	0.0651
$T_{max} > 1.3$ and $T_{min} > 1.3$	0.9698	0.165	−0.0164	0.0043	0.1349	−0.1254
$T_{max} < 5.0$ and $T_{min} \leq 0.2$	1.2109	−1.0703	1.9603	0.8964	1.074	0.3267
$T_{max} \geq 5.0$ and $T_{min} \leq 0.2$	0.7595	0.7033	−0.0454	−0.4994	−0.0135	0.0658

equation.

7. Engineering application: seismic hazard curves using V_{EI} and V_{EIavg}

Currently, the majority of GMPEs are established to predict the spectral acceleration, S_a (T_1), measured at the fundamental period of a structure. S_a (T_1) is the ground motion intensity measure most used in PSHA and probabilistic seismic demand analyses. However, this intensity measure has certain limitations [31,61–63]. As a result, advanced seismic intensity measures have emerged, aiming to overcome the drawbacks associated with traditional measures. One such example is intensity measures based on energy concepts. Unfortunately, the use of these intensity measures is limited due to the lack of appropriate GMPEs.

In relation to the above, the procedure presented in this study enables the development of GMPEs, facilitating the estimation of PSHA using V_{EI}, as demonstrated in the subsequent sections. Furthermore, the proposed GMPEs and the correlation model described previously are valuable for utilizing IMs that involve combinations of spectral values across different vibration periods, such as the geometric mean of spectral values over a period range. For instance, the geometric mean of

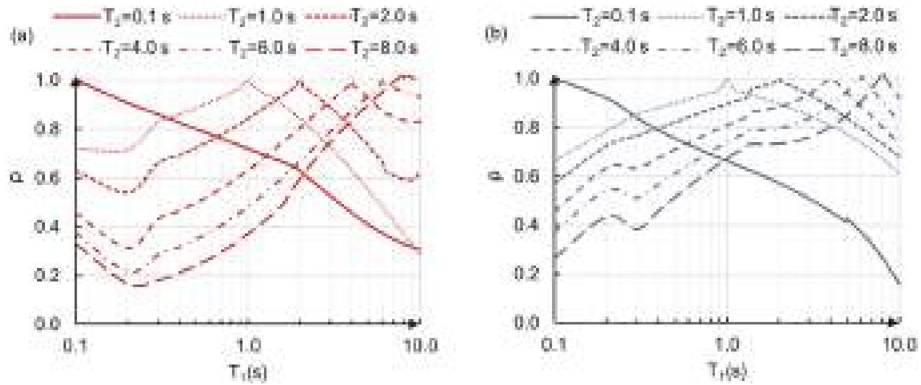

Fig. 10. Plots of correlation coefficients versus T_1, for several T_2 values. Using predictive correlation equations: (a) Interplate and (b) Intraslab.

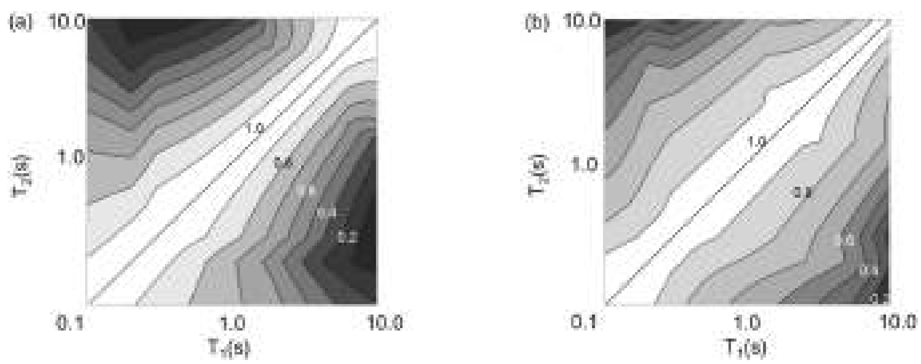

Fig. 11. Contours of correlation coefficients between T_1 and T_2. Using the predictive correlation equation for: (a) Interplate, and (b) Intraslab events.

spectral accelerations, Sa_{avg}, has been successfully employed to predict the response of structures affected by excitation at different vibration periods [59]. Several studies have compared the efficiency and sufficiency of Sa_{avg} with respect to $Sa(T_1)$, revealing improved prediction of structural response when using Sa_{avg} [30,64,65]. Therefore, extending this concept, it becomes feasible to predict the geometric mean of V_{EI} spectral values over a period range, denoted as V_{EIavg}.

In the following, the mean annual rates of exceedance (hazard curves) of V_{EI} and V_{EIavg} is estimated. The discussion regarding the advantages of employing these intensity measures is beyond the scope of this section. In what follows, the development to define the expected value and the variance of the natural logarithm of V_{EIavg} is presented; a similar approach for Sa_{avg} can be found elsewhere [29,59]. In first place, V_{EIavg} is defined as:

$$V_{EI\,avg}(T_1 \ldots T_N) = \left(\prod_{i=1}^{N} V_{EI}(T_i) \right)^{1/N} \tag{22}$$

where V_{EIavg} denotes the equivalent velocity of input energy averaged over a period range, $T_1 \ldots T_N$, at N numbers of periods. Next, applying natural logarithm, it becomes:

$$ln\ V_{EI\,avg}(T_1 \ldots T_N) = \frac{1}{N} \sum_{i=1}^{N} ln[V_{EI}(T_i)] \tag{23}$$

Then, the expected value and the variance of lnV_{EIavg} can be expressed as:

$$E\left[ln\ V_{EI\,avg}(T_1 \ldots T_N)\right] = \frac{1}{N} \sum_{i=1}^{N} E\{ln[V_{EI}(T_i)]\} \tag{24}$$

$$Var\left[ln\ V_{EI\,avg}(T_1 \ldots T_N)\right] = \frac{1}{N^2} \sum_{i=1}^{N} \sum_{j=1}^{N} \left[\rho_{ln[V_{EI}(T_i)],\ln\left[V_{EI}(T_j)\right]} \sigma_{\ln\left[V_{EI}(T_i)\right]} \sigma_{\ln\left[V_{EI}(T_j)\right]}\right] \tag{25}$$

where the $ln[V_{EI}(T_i)]$ values can be estimated with the proposed GMPEs (Eqs. (12) and (13)), and $\rho\ ln[V_{EI}(T_i)], ln[V_{EI}(T_j)]$ represents the correlation between V_{EI} spectral values at periods T_i and T_j, which can be computed using Eq. (21). Thus, a customized attenuation model for V_{EIavg} has been established, and all these equations are enough to describe the complete distribution of V_{EIavg}.

Fig. 12 presents the mean annual rate of exceedance of V_{EI} and V_{EIavg} for $T_1 = 2.0$s (the range of periods for V_{EIavg} was taken from T_1 to $2T_1$) corresponding to two accelerometer stations installed in Mexico City: CU and Ministry of Communications and Transportation of Mexico (SCT) (Fig. 12a and b, respectively). The CU site is within the hill zone area (firm ground), and the SCT station is in the lake-bed zone area (soft soil) of Mexico City. The hazard curves for both intensity measures, V_{EI} and V_{EIavg}, were estimated using the GMPEs and the correlation model proposed in this study. It is important to note that the hazard curves for SCT station were calculated with the formulation introduced by Esteva [66], which enables the estimation of a hazard curve at a recipient site based on a known hazard curve at a reference site. In this case, CU was selected as the reference site.

8. Conclusions

Nowadays, new approaches for earthquake-resistant design have arisen to improve and overcome the shortcomings of conventional earthquake-resistant design procedures. Such as the case of earthquake-resistant design methodologies based on energy concepts. These methodologies focus on providing structures with an appropriate capacity to dissipate the energy imparted by earthquakes during ground motions.

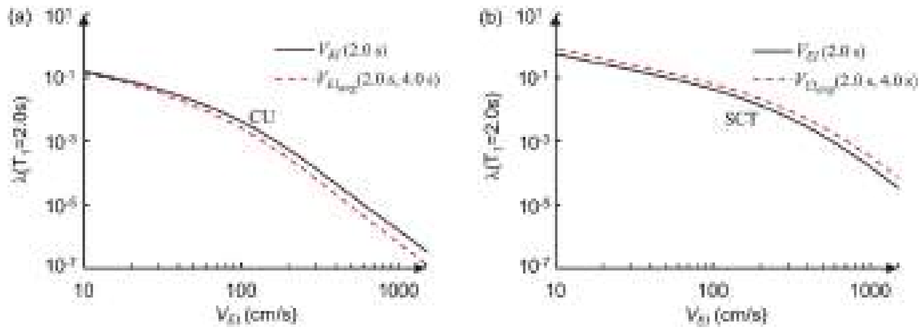

Fig. 12. Mean annual rate of exceedance (λ) for V_{EI} and V_{EIavg} at: a) CU accelerometer station (firm ground) and b) SCT accelerometer station (soft soil).

Consequently, it becomes crucial to define the earthquake input energy transmitted to structures.

- Ground motion prediction equations are proposed to estimate the response spectra (5% of critical damping) for the equivalent velocity of input energy (V_{EI}) at sites located within the hill zone (firm ground) of Mexico City, considering interplate and, alternatively, intraslab earthquakes. For this purpose, a methodology based on the combination of an existing relationship between the Fourier amplitude spectrum and the elastic input energy spectrum in conjunction with a Bayesian regression technique is presented. By comparing the exact V_{EI} response spectra with those estimated with the proposed GMPEs, it is concluded that the procedure provides adequate results for both types of seismic events.
- The proposed GMPEs describe the probability distribution of V_{EI} spectral values at a single period; however, they do not provide any information about the joint distribution of V_{EI} spectral values at multiple periods. Having that information, the applicability of the proposed predicted equations can be extended. In this regard, the correlation coefficients between spectral values are useful to define the joint distribution of spectral values at different periods.
- Hence, the correlation coefficients between spectral V_{EI} values at multiple vibration periods are estimated using interplate and intraslab seismic ground motions recorded at the firm ground in Mexico City, along with the GMPEs proposed in this study. The results reveal distinct spreading patterns of the correlation coefficients when considering interplate and intraslab ground motion records. This finding underscores the strong dependence of correlation coefficients on the rupture mechanism, consistent with previous studies on correlation coefficients between spectral acceleration values.
- Consequently, a mathematical expression is proposed to estimate the correlation coefficients between V_{EI} spectral values at multiple periods for both interplate and intraslab earthquakes on the firm ground of Mexico City.
- Finally, the GMPEs developed in this study are employed to estimate the mean annual rate of exceedance (hazard curve) of V_{EI} and V_{EIavg} at two sites representing the firm ground and soft soil of Mexico City. To estimate the hazard curve associated with V_{EIavg}, the proposed correlation model is utilized.

Author statement

Edén Bojórquez: Conceptualization, Methodology. **Sonia E. Ruiz:** Methodology, Supervision, Resources. **Ali Rodríguez-Castellanos:** Investigation, Formal analysis, Writing-Original draft preparation. **Miguel A. Orellana:** Software, Writing-Original draft preparation. **Alfredo Reyes-Salazar:** Writing - Review & Editing. **Juan Bojórquez:** Writing - Review & Editing.

Declaration of competing interest

The authors declare that they have no known competing financial interests or personal relationships that could have appeared to influence the work reported in this paper.

Data availability

Data will be made available on request.

Acknowledgments

The present study was supported by CONACyT and DGAPA-UNAM under the project Ciencia de Frontera CF-2023-G-1636 and PAPIIT-IN100423, respectively. The corresponding author thanks CONACyT for the support given during his graduate studies. The authors thank The Strong Motion Network of the Institute of Engineering at UNAM, Mexico (RAII-UNAM) for providing the seismic records.

References

[1] Federal Emergency Management Agency (FEMA). In: Prestandard and commentary for the seismic rehabilitation of buildings, Rep. No. FEMA-356. Washington, DC: Federal Emergency Management Agency; 2000.
[2] American Society of Civil Engineers (ASCE). Minimum design loads and associated criteria for buildings and other structures. Reston, VA: American Society of Civil Engineers; 2017. https://doi.org/10.1061/9780784414248.
[3] Gobierno de la Ciudad de Mexico (GCDMX). Normas técnicas complementarias para diseño por sismo. Ciudad de México: Gobierno de la Ciudad de México; 2020.
[4] Liu BQ, Liu M, Li YB. Research and development of performance based seismic design theory. In: Proceedings of the 13th World conferece on earthquake engineering. Vancouver, B.C.; 2004.
[5] Priestley MJN, Calvi GM, Kowalsky MJ. Displacement-based seismic design of structures. Pavia, Italy: IUSS Press; 2007.
[6] Bojórquez E, Terán-Gilmore A, Ruiz SE, Reyes-Salazara A. Evaluation of structural reliability of steel frames: interstory drift versus plastic hysteretic energy. Earthq Spectra 2011;27(3):661–82. https://doi.org/10.1193/1.3609856.
[7] Benavent-Climent A, López-Almansa F, Bravo-González DA. Design energy input spectra for moderate-to-high seismicity regions based on Colombian earthquakes. Soil Dynam Earthq Eng 2010;30:1129–48. https://doi.org/10.1016/j.soildyn.2010.04.022.
[8] Quinde P, Reinoso E, Terán-Gilmore A. Inelastic seismic energy spectra for soft soils: application to Mexico City. Soil Dynam Earthq Eng 2016;89:198–207. https://doi.org/10.1016/j.soildyn.2016.08.004.
[9] Housner GW. Spectrum intensities of strong-motion earthquakes. In: Proceedings of the symposium on earthquake and blast effects on structures. Los Angeles, CA; 1952. p. 20–36.
[10] Akiyama H. Earthquake resistant design based on the energy concept. In: Proceedings of the 9th World conferece on earthquake engineering. Kyoto: Tokyio; 1988.
[11] Uang C-M, Bertero VV. Evaluation of seismic energy in structures. Earthq Eng Struct Dynam 1990;19:77–90. https://doi.org/10.1002/eqe.4290190108.
[12] Fajfar P, Vidic T. Consistent inelastic design spectra: hysteretic and input energy. Earthq Eng Struct Dynam 1994;23:523–37. https://doi.org/10.1002/eqe.4290230505.
[13] Chou CC, Uang CM. Establishing absorbed energy spectra - an attenuation approach. Earthq Eng Struct Dynam 2000;29:1441–55. https://doi.org/10.1002/1096-9845(200010)29:10<1441::AID-EQE967>3.0.CO;2-E.
[14] Decanini LD, Mollaioli F. An energy-based methodology for the assessment of seismic demand. Soil Dynam Earthq Eng 2001;21:113–37. https://doi.org/10.1016/S0267-7261(00)00102-0.

[15] Manfredi G. Evaluation of seismic energy demand. Earthq Eng Struct Dynam 2001; 30(4):485–99. https://doi.org/10.1002/eqe.17.
[16] Benavent-Climent A, Pujades LG, López-Almansa F. Design energy input spectra for moderate-seismicity regions. Earthq Eng Struct Dynam 2002;31:1151–72. https://doi.org/10.1002/eqe.153.
[17] Amiri GG, Darzi GA, Khanzadi M. Earthquake duration and damping effects on input energy. Int J Civ Eng 2007;5:14–29.
[18] Uang C, Bertero VV. Evaluation of seismic energy in structures. Earthq Eng Struct Dynam 1990;19:77–90. https://doi.org/10.1002/eqe.4290190108.
[19] Decanini LD, Mollaioli F. Formulation of elastic earthquake input energy spectra. Earthq Eng Struct Dynam 1998;27:1503–22. https://doi.org/10.1002/(sici)1096-9845(199812)27:12<1503::aid-eqe797>3.3.co;2-1522.
[20] Chai YH, Fajfar P. A procedure for estimating input energy spectra for seismic design. J Earthq Eng 2000;4:539–61. https://doi.org/10.1080/13632460009350382.
[21] Chapman MC. On the use of elastic input energy for seismic hazard analysis. Earthq Spectra 1999;15:607–35. https://doi.org/10.1193/1.1586064.
[22] Gong M, Xie L. Study on comparison between absolute and relative input energy spectra and effects of ductility factor. Acta Seismol Sin 2005;27:717–26. https://doi.org/10.1007/s11589-005-0099-4.
[23] Joyner WB, Boore DM. Methods for regression analysis of strong-motion data. Bull Seismol Soc Am 1993;83:469–87. https://doi.org/10.1785/BSSA0830020469.
[24] Danciu L, Tselentis GA. Engineering ground-motion parameters attenuation relationships for Greece. Bull Seismol Soc Am 2007;97:162–83. https://doi.org/10.1785/0120050087.
[25] Cheng Y, Lucchini A, Mollaioli F. Proposal of new ground-motion prediction equations for elastic input energy spectra. Earthq Struct 2014;7:485–510. https://doi.org/10.12989/eas.2014.7.4.485.
[26] Alıcı FS, Sucuoğlu H. Prediction of input energy spectrum: attenuation models and velocity spectrum scaling. Earthq Eng Struct Dynam 2016;45:2137–61. https://doi.org/10.1002/eqe.2749.
[27] Bazurro P, Cornell CA. Vector-valued probabbilistic seismic hazard analysis (VPSHA). In: Proceedings of the National Conference on earthquake engineering. Boston, MA; 2002.
[28] Baker JW, Cornell CA. Correlation of response spectral values for multicomponent ground motions. Bull Seismol Soc Am 2006;96:215–27. https://doi.org/10.1785/0120050060.
[29] Baker JW, Cornell CA. Spectral shape, epsilon and record selection. Earthq Eng Struct Dynam 2006;35:1077–95. https://doi.org/10.1002/eqe.571.
[30] Kohrangi M, Kotha SR, Bazzurro P. Ground-motion models for average spectral acceleration in a period range: direct and indirect methods. Bull Earthq Eng 2018; 16:45–65. https://doi.org/10.1007/s10518-017-0216-5.
[31] Baker JW, Cornell CA. A vector-valued ground motion intensity measure consisting of spectral acceleration and epsilon. Earthq Eng Struct Dynam 2005;34:1193–217. https://doi.org/10.1002/eqe.474.
[32] Baker JW. Conditional mean spectrum: tool for ground-motion selection. J Struct Eng 2011;137:322–31. https://doi.org/10.1061/(ASCE)ST.1943-541X.0000215.
[33] Singh SK, Cruz-Atienza V, Pérez-Campos X, Iglesias A, Hjörleifsdóttir V, Reinoso E, et al. Deadly intraslab Mexico earthquake of 19 September 2017 (Mw 7.1): ground motion and damage pattern in Mexico City. Seismol Res Lett 2018;89:2193–203. https://doi.org/10.1785/0220180159.
[34] Ordaz M, Huerta B, Reinoso E. Exact computation of input-energy spectra from Fourier amplitude spectra. Earthq Eng Struct Dynam 2003;32:597–605. https://doi.org/10.1002/eqe.240.
[35] Takewaki I. Frequency domain modal analysis of earthquake input energy to highly damped passive control structures. Earthq Eng Struct Dynam 2004;33:575–90. https://doi.org/10.1002/eqe.361.
[36] Campbell KW. Near-source attenuation of peak horizontal acceleration. Bull Seismol Soc Am 1981;71:2039–70. https://doi.org/10.1785/BSSA0710062039.
[37] Joyner WB, Boore DM. Peak horizontal acceleration and velocity from strong-motion records including records from the 1979 imperial valley, California, earthquake. Bull Seismol Soc Am 1981;71:2011–38. https://doi.org/10.1785/BSSA0710062011.
[38] Abrahamson NA, Youngs RR. A stable algorithm for regression analyses using the random effects model. Bull Seismol Soc Am 1992;82:505–10. https://doi.org/10.1785/BSSA0820010505.
[39] Ordaz M, Singh SK, Arciniega A. Bayesian attenuation regressions: an application to Mexico city. Geophys J Int 1994;117:335–44. https://doi.org/10.1111/j.1365-246X.1994.tb03936.x.
[40] Jaimes MA, Reinoso E, Ordaz M. Comparison of methods to predict response spectra at instrumented sites given the magnitude and distance of an earthquake. J Earthq Eng 2006;10:887–902. https://doi.org/10.1080/13632460609350622.
[41] Arroyo D, Ordaz M. Multivariate bayesian regression analysis applied to ground-motion prediction equations, part 2: numerical example with actual data. Bull Seismol Soc Am 2010;100:1568–77. https://doi.org/10.1785/0120090320.
[42] Ordaz M, Reyes C. Earthquake hazard in Mexico City: observations versus computations. Bull Seismol Soc Am 1999;89:1379–83. https://doi.org/10.1785/BSSA0890051379.
[43] García D, Singh SK, Herraíz M, Ordaz M, Pacheco JF. Inslab earthquakes of Central Mexico: peak ground-motion parameters and response spectra. Bull Seismol Soc Am 2005;95:2272–82. https://doi.org/10.1785/0120050072.
[44] Jaimes MA, Ramirez-Gaytan A, Reinoso E. Ground-motion prediction model from intermediate-depth intraslab earthquakes at the hill and lake-bed zones of Mexico city. J Earthq Eng 2015;19:1260–78. https://doi.org/10.1080/13632469.2015.1025926.
[45] Aki K. Scaling law of seismic spectrum. J Geophys Res 1967;72:1217–31. https://doi.org/10.1029/JZ072i004p01217.
[46] Brune JN. Tectonic stress and the spectra of seismic shear waves from earthquakes. J Geophys Res 1970;75:4997–5009. https://doi.org/10.1029/JB075i026p04997.
[47] Rodríguez-Pérez Q, Márquez-Ramírez VH, Zúñiga FR, Plata-Martínez R, Pérez-Campos X. The Mexican earthquake source parameter database: a new resource for earthquake physics and seismic hazard analyses in Mexico. Seismol Res Lett 2018; 89:1846–62. https://doi.org/10.1785/0220170250.
[48] García D, Singh SK, Herráiz M, Pacheco JF, Ordaz M. Inslab earthquakes of Central Mexico: Q, source spectra, and stress drop. Bull Seismol Soc Am 2004;94:789–802. https://doi.org/10.1785/0120030125.
[49] García D, Singh SK, Herraiz M, Ordaz M, Pacheco JF, Cruz-Jiménez H. Influence of subduction zone structure on coastal and inland attenuation in Mexico. Geophys J Int 2009;179:215–30. https://doi.org/10.1111/j.1365-246X.2009.04243.x.
[50] Reyes C. El estado límite de servicio en el diseño sísmico de edificios. PhD Thesis. México: UNAM; 1999 (in Spanish).
[51] Atkinson GM, Mereu RF. The shape of ground motion attenuation curves in southeastern Canada. Bull Seismol Soc Am 1992;82:2014. https://doi.org/10.1785/BSSA0820052014. –31.
[52] Atkinson GM, Boore DM. Ground-motion relations for eastern North America. Bull Seismol Soc Am 1995;85:17–30. https://doi.org/10.1785/BSSA0850010017.
[53] Singh SK, Ordaz M, Pérez-Campos X, Iglesias A. Intraslab versus interplate earthquakes as recorded in Mexico City: implications for seismic hazard. Earthq Spectra 2015;31:795–812. https://doi.org/10.1193/110612EQS324M.
[54] Rodríguez-Castellanos A. Evaluación del peligro sísmico en algunos sitios del valle de México, utilizando la medida de intensidad I_{Np}. PhD Thesis. México: UNAM; 2021 (in Spanish).
[55] Arroyo D, García D, Ordaz M, Mora MA, Singh SK. Strong ground-motion relations for Mexican interplate earthquakes. J Seismol 2010;14:769–85. https://doi.org/10.1007/s10950-010-9200-0.
[56] Jayaram N, Baker JW. Statistical tests of the joint distribution of spectral acceleration values. Bull Seismol Soc Am 2008;98:2231–43. https://doi.org/10.1785/0120070208.
[57] Rodríguez-Castellanos A, Ruiz SE, Bojórquez E, Reyes-Salazar A. Influence of spectral acceleration correlation models on conditional mean spectra and probabilistic seismic hazard analysis. Earthq Eng Struct Dynam 2020. https://doi.org/10.1002/eqe.3331. eqe.3331.
[58] Carlton B, Abrahamson N. Issues and approaches for implementing conditional mean spectra in practice. Bull Seismol Soc Am 2014;104:503–12. https://doi.org/10.1785/0120130129.
[59] Baker JW, Jayaram N. Correlation of spectral acceleration values from NGA ground motion models. Earthq Spectra 2008;24:299–317. https://doi.org/10.1193/1.2857544.
[60] Hong HP, Pozos-Estrada A, Gomez R. Orientation effect on ground motion measurement for Mexican subduction earthquakes. Earthq Eng Eng Vib 2009;8:1–16. https://doi.org/10.1007/s11803-009-8155-z.
[61] Cordova PP, Deierlein GG, Mehanny SSF, Cornell CA. Development of a two-parameter seismic intensity measure and probabilistic design procedure. J Eng Appl Sci 2001;51:233–52.
[62] Tothong P, Luco N. Probabilistic seismic demand analysis using advanced ground motion intensity measures. Earthq Eng Struct Dynam 2007;36:1837–60. https://doi.org/10.1002/eqe.696.
[63] Cheng Y, Lucchini A, Mollaioli F. Ground-motion prediction equations for constant-strength and constant-ductility input energy spectra. Bull Earthq Eng 2020;18:37–55. https://doi.org/10.1007/s10518-019-00725-x.
[64] Kazantzi AK, Vamvatsikos D. Intensity measure selection for vulnerability studies of building classes. Earthq Eng Struct Dynam 2015;44:2677–94. https://doi.org/10.1002/eqe.2603.
[65] Kohrangi M, Bazzurro P, Vamvatsikos D, Spillatura A. Conditional spectrum-based ground motion record selection using average spectral acceleration. Earthq Eng Struct Dynam 2017;46:1667–85. https://doi.org/10.1002/eqe.2876.
[66] Esteva L. Regionalización sísmica de México para fines de ingeniería, SID246. Inst Ing UNAM; 1970. p. 229–46.